Available online at www.sciencedirect.com
ScienceDirect
Polymer 47 (2006) 6673–6683
polymer
www.elsevier.com/locate/polymer

Nanoscale structure of SAN–PEO–SAN triblock copolymers synthesized by atom transfer radical polymerization

Michal Shach-Caplan [a], Michael S. Silverstein [a,*], Havazelet Bianco-Peled [b], Nicolay V. Tsarevsky [c], Beth M. Cooper [c], Krzysztof Matyjaszewski [c]

[a] *Department of Materials Engineering, Technion – Israel Institute of Technology, Haifa 32000, Israel*
[b] *Department of Chemical Engineering, Technion – Israel Institute of Technology, Haifa 32000, Israel*
[c] *Department of Chemistry, Carnegie Mellon University, Pittsburgh, PA 15213, USA*

Received 15 June 2006; received in revised form 11 July 2006; accepted 12 July 2006
Available online 14 August 2006

Abstract

Low molecular weight triblock copolymers (TBCs) with poly(styrene-*co*-acrylonitrile) (SAN) end-blocks and poly(ethylene oxide) (PEO), poly(propylene oxide) (PPO) or polycaprolactone (PCL) mid-blocks were synthesized using atom transfer radical polymerization (ATRP). The influence of molecular weight, composition (mid-block mole fraction), and interaction parameter on the crystallinity and on the formation of an ordered nanoscale phase-separated structure was investigated using thermal analysis, X-ray scattering, and electron microscopy. The TBCs with PEO mole fractions of over 0.5 exhibited PEO crystallinities of around 40% (compared to 72% for the PEO homopolymer) and lamellar nanoscale periodicities of around 176 Å (compared to 143 Å for the PEO homopolymer). The TBCs with PEO, PCL or PPO mole fractions of less than 0.5 exhibited relatively low crystallinities and did not exhibit ordered structures. These results emphasize the importance of the mid-block mole fraction in determining the ability to form an ordered nanoscale structure through mid-block crystallization. The ordered structure disappeared on heating the TBCs above the mid-block melting point, but below the SAN glass transition temperature. The crystallinity was reduced significantly in TBCs that were annealed or cast from a solvent.

Keywords: Triblock copolymer; Atom transfer radical polymerization; Poly(ethylene oxide)

1. Introduction

Controlled/'living' radical polymerizations (CRPs) such as atom transfer radical polymerization (ATRP) can overcome many of the limitations of other living polymerization reactions (only a small number of monomers can be used, the reactions are sensitive to moisture, and two or more monomers cannot be randomly copolymerized) and provide a method to maximize the potential of living polymerizations (hundreds of monomers are available, two or more monomers can be randomly copolymerized, emulsions or suspensions can be used) [1]. The control of the polymerization afforded by ATRP is a result of the formation of radicals that can grow, but are reversibly deactivated to form dormant species [2,3]. Reactivation of the dormant species allows the polymer chains to grow again, only to be deactivated later. Such a process results in a polymer chain that slowly, but steadily, grows and has a well-defined end group (for ATRP that end group is usually an alkyl halide) [4,5]. Although other controlled radical polymerization systems have been reported by various groups [6,7], ATRP remains the most powerful, versatile, simple, and inexpensive. ATRP produces polymers with very low polydispersities and provides extensive control of molecular architecture using a wide range of monomers [8]. The use of ATRP for the synthesis of segmented and gradient copolymers is especially important. A variety of gradient, block and graft copolymers with novel compositions, macromolecular architectures

* Corresponding author. Tel./fax: +972 4 829 4582.
E-mail address: michaels@tx.technion.ac.il (M.S. Silverstein).

0032-3861/$ - see front matter © 2006 Elsevier Ltd. All rights reserved.
doi:10.1016/j.polymer.2006.07.019

and functional end groups have been prepared [9,10]. ATRP has been used successfully to synthesize well-defined polymers with molecular weights ranging from 1000 to 100,000 g/mol. However, termination and other side reactions also occur, and they become more prominent as the molecular weight of the polymer increases [3,11]. Acrylonitrile (AN) is one of the monomers successfully polymerized by ATRP, and both homopolymers [12] and random copolymers [13] have been reported.

A great deal of research has been focused on the nanoscale structures of high molecular weight triblock copolymers (TBCs) [14]. However, little is known regarding the nanoscale structures in lower molecular weight TBCs that contain crystallizable mid-blocks (MB). Block copolymers can spontaneously order into a variety of nanoscale structural elements that impart complementary properties to multifunctional materials [15]. The objectives of this research were to study the nanoscale structures in low molecular weight TBCs containing crystallizable mid-blocks and glassy end-blocks. These polymers contain two driving forces for nanoscale ordering, the first is phase separation between the polymer blocks and the second is the crystallization of the mid-block. The nanoscale structure in semicrystalline–rubbery–semicrystalline triblock copolymers has been shown to be strongly dependent on whether segregation was induced by crystallization or by phase separation in the melt [16]. Unlike the semicrystalline–rubbery–semicrystalline triblock copolymers, the crystallization in these TBCs will be further limited since the crystallizable block is the mid-block, rather than the end-block, and since the glass transition temperature of the amorphous block is higher than, rather than lower than, the crystallization temperature of the semicrystalline block. Polyethylene crystallinity was reduced to between 15 and 20% in a TBC with a crystallizable polyethylene mid-block and glassy poly(cyclohexylethylene) end-blocks [17].

TBCs with amorphous poly(styrene-*co*-acrylonitrile) (SAN) end-blocks and crystallizable poly(ethylene oxide) (PEO) mid-blocks were synthesized using ATRP [13]. PEO mid-blocks with both relatively low and relatively high number average molecular weights (M_n) were synthesized. In addition, triblock copolymers with poly(ε-caprolactone) (PCL) and poly(propylene oxide) (PPO) mid-blocks were investigated. PEO is a biocompatible and non-immunogenic water-soluble semicrystalline polymer [18]. Various polymer systems based on PEO and PCL have been the subject of studies in the area of biomedical applications such as drug delivery systems.

In this research the nanoscale structure of these block copolymers was characterized using complementary thermal analysis, spectroscopic and microscopic techniques. The effects of molecular weight, relative block size, polymer–polymer compatibility and processing history (annealing, solvent casting) on the nanoscale structure were studied. The materials in this research include a set of TBCs with different molecular weights (but similar compositions), a set of TBCs with different compositions (but similar molecular weights), and a set of TBCs with different mid-block polymers (but similar molecular weights and compositions).

2. Experimental section

2.1. Synthesis

The various homopolymers and triblock copolymers synthesized are listed in Table 1.

2.1.1. Synthesis of polymeric macro-radicals for ATRP

The PEO macroinitiator was synthesized through the esterification of the polymeric alcohol, dihydroxy-terminated poly(ethylene oxide) with 2-bromopropionic acid in the presence of dicyclohexylcarbodiimide (DCC) and catalytic amounts of 4-(*N*,*N*-dimethylamino) pyridine (4-DMAP) in methylene chloride [13,19]. The PPO and PCL macroinitiators were synthesized in a similar manner, through the esterification of dihydroxypoly(propylene oxide) and dihydroxypoly-(ε-caprolactone), respectively. A detailed procedure for the esterification and for the preparation of SAN is reported elsewhere [13].

Table 1
Molecular weights, compositions, $\chi_{ij}N/2$, transition temperatures and crystallinities

	SAN M_n	MB M_n	PDI	N_{SAN}	N_{MB}	x_{MB}	$\chi_{ij}N/2$	T_m (°C)	X_{MB} (%)	T_g (°C)
SAN1	8300	–	1.08	97	–	–	–	–	–	92
PEO1	–	2500	1.04	–	57	–	–	56	63	–
PEO1-a	3200	2500	1.09	38	57	0.43	0.056	50	4	–
PEO1-b	5050	2500	1.10	59	57	0.32	0.075	72	7	–
PEO1-c	8600	2500	1.11	101	57	0.22	0.11	86	22	–
PEO1-d	10,850	2500	1.14	127	57	0.18	0.13	63	23	–
PEO2	–	6100	1.05	–	138	–	–	64	72	–
PEO2-a	3250	6100	1.09	38	138	0.64	0.092	58	42	–
PEO2-b	4800	6100	1.10	56	138	0.55	0.11	52	43	–
PEO2-c	7550	6100	1.11	89	138	0.44	0.14	85	12	–
PEO3-a	5700	11,500	1.05	67	261	0.66	0.17	63	38	–
PPO1-a	3750	1470	1.16	44	25	0.22	2.9	70	26	–
PCL1-a	3740	3360	1.21	44	29	0.25	5.8	58	13	−51

2.1.2. Synthesis of triblock copolymers by ATRP

$PEO(BP)_2$ (2.5×10^{-3} mol), 4.9 mL (7.45×10^{-2} mol) of acrylonitrile (AN), and 14.5 mL (1.27×10^{-1} mol) of styrene were mixed together in a Schlenk flask. The monomers were chosen to yield SAN with 37 mol% AN (azeotropic monomer feed composition). The resulting solution was degassed by four freeze-pump-thaw cycles, the flask was filled with nitrogen, and, while the mixture was immersed in liquid nitrogen, 0.36 g (2.5×10^{-3} mol) of CuBr and 0.78 g (5.0×10^{-3} mol) of bipyridine were added. The flask was then closed with a glass stopper, evacuated and back-filled with nitrogen for four times. The mixture was melted and a brown solution containing a small amount of solid catalyst was formed. The polymerization was carried out at 80 °C. The polymers were dissolved in tetrahydrofuran (THF), precipitated in methanol, and dried. Copolymers with a higher degree of polymerization in the SAN blocks were prepared by adjusting the ratio of the monomers to the initiator.

2.2. Molecular weight

Size exclusion chromatography (SEC) measurements were conducted using THF as the eluent (flow rate 1 mL/min, 30 °C), with a series of three Styragel columns (10^5, 10^3 and 100 Å; Polymer Standard Services) and a Waters 2410 differential refractometer. Diphenyl ether was used as the flow rate marker. Calibration based on polystyrene standards was applied for the determination of the relative molecular weights of all the polymers, including the macroinitiators. The M_n of the mid-blocks, the M_n of the SAN end-blocks, and the polydispersity index (PDI, the weight average molecular weight divided by M_n) are listed in Table 1. The PDIs are around 1.1, reflecting a narrow distribution of molecular weights.

Among the TBCs synthesized were two sets of triblock copolymers, one based on PEO mid-blocks of M_n 2500 g/mol and the other based on PEO mid-blocks of M_n 6100 g/mol, each with various SAN M_n (Table 1). The M_n of the TBCs is the sum of the mid-block M_n and twice the SAN end-block M_n. The degrees of polymerization for the SAN end-block and for the mid-block, N_{SAN} and N_{MB}, respectively, are also listed in Table 1. The degrees of polymerization were calculated by dividing M_n by the molecular weight of the repeat unit, M_0 (listed in Table 2). The total degree of polymerization for the TBCs, N, is $N_{MB} + 2N_{SAN}$. The mole fraction of the mid-block polymer, x_{MB}, is N_{MB}/N.

2.3. Thermal analysis

Differential scanning calorimetry (DSC) in nitrogen was used to characterize the glass transition temperatures (T_gs), the PEO, PPO, and PCL melting points (T_ms) and the PEO, PPO, and PCL crystallinities (Mettler DSC-821 calorimeter). After comparing the thermograms from samples run at a few different heating rates (5, 10, and 20 °C/min) it was determined that 20 °C/min provided the most unambiguous results. The samples were initially cooled to −100 °C at 50 °C/min and then heated immediately to 120 °C ('first heat'), cooled immediately to −100 °C, and then heated again immediately to 120 °C ('second heat'), all at 20 °C/min. The extent of PEO crystallinity has been related to the extent of undercooling [20]. Since the DSC samples were all cooled to −100 °C, all the samples had a similar undercooling history.

The molar melting enthalpy per mole mid-block polymer was calculated by dividing the measured heat of melting per mass sample by the mass fraction of mid-block polymer and multiplying by the mid-block M_0. The degree of crystallinity, X_{MB}, was calculated by dividing the molar melting enthalpy per mole mid-block polymer by the heat of fusion for 100% crystallinity, ΔH_f (Table 2) [21,22].

The as-synthesized polymers were characterized by the first heat in the DSC. The effects of the annealing that takes place during the first heat in the DSC were investigated by the second heat in the DSC. The effects of solution processing were investigated by casting the polymer into a DSC crucible, drying, and then running the DSC experiment.

2.4. Structural analysis

Transmission electron microscopy (TEM) samples were prepared by ultra cryomicrotomy (Reichert-Jung, FC 4E, USA) at −50 °C. Conventional TEM was performed on a JEOL 2000FX operated at 200 kV. Wide-angle X-ray scattering (WAXS) was performed at room temperature using Cu Kα radiation in the angular (2θ) range of 10° to 40°. Powders were placed in a poly(methyl methacrylate) (PMMA) sample holder. The effects of solution processing were investigated by casting onto $LiNbO_3$. The scattering curves are shifted vertically as a visual aid.

Small angle X-ray scattering (SAXS) was performed at room temperature with Cu Kα radiation using a compact Kratky Camera (Anton Paar) having a linear position-sensitive detector system with phase-height discrimination (Raytech)

Table 2
Polymer properties and interaction parameters

	M_0 (g/mol)	ρ (g/cc)	v (cc/mol)	ΔH_f (kJ/mol)	T_g (°C)	T_m (°C)	δ (MPa)$^{0.5}$	χ_{ij}	χ_{ijk}
PS	104.1	1.05	99.2	–	90	–	18.6	–	–
PAN	53.1	1.17	45.4	–	90	–	25.3	–	–
SAN	85.2	1.08[a]	79.1	–	90[a]	–	20.0[a]	–	–
PEO	44.0	1.13	38.9	11.7	−63	66	19.8	0.0009	−0.052
PPO	58.1	1.00	58.1	8.4	−75	75	18.5	0.050	0.0002
PCL	114.1	1.04	109.8	15.5	−62	60	18.2	0.099	0.085

[a] The SAN M_0, ρ, and δ were calculated using rules of mixtures. The SAN T_g was calculated using the Fox equation.

coupled to a multichannel analyzer (Nucleus). The entrance slit to the collimation block was 30 μm, and the slit length delimiters were set at 15 mm. The sample-to-detector distance was 26.4 cm. Sample powders were taped directly to the sample holder. The effects of solution processing were investigated by casting onto polyimide films. The scattering curves were corrected for sample absorption. The constant background, determined using a Porod plot, was subtracted. The correction for the effects of the geometry of a slit-collimated incident beam (desmearing) was performed using an indirect Fourier transformation procedure [23]. The scattering curves are shifted vertically as a visual aid.

When the SAXS data did not indicate the presence of a lamellar structure in the TBCs, a Debye correlation function was used to fit the SAXS data:

$$I(h) = \frac{I(0)}{\left(1 + h^2\xi^2\right)^2} \tag{1}$$

where h is the scattering vector ($h = 4\pi \sin\theta/\lambda$ where 2θ and λ are the scattering angle and the wavelength, respectively), ξ is the correlation length used to describe the length scale associated with scattering from a two-phase disordered system and $I(h)$ is the one-dimensional scattering intensity and $I(0)$ is the intensity for $h = 0$.

2.5. Processing

The annealed polymers are those that were heated in the DSC to a temperature of 120 °C during the first heat and then characterized during the second heat, as described above. The solvent-cast polymers were dissolved in either THF or chloroform ($CHCl_3$) and cast onto a polyimide film (for SAXS), $LiNbO_3$ (three times in succession for WAXS), or into an aluminum crucible (for DSC). One set of cast films was dried in a vacuum oven at 25 °C for 2 h and another set was dried in a vacuum oven at 150 °C for 2 h.

3. Results and discussion

3.1. Polymer properties and interaction parameters

Typical physical and thermal properties from the literature for PEO, PPO, PCL, polystyrene (PS), and polyacrylonitrile (PAN) homopolymers as well as for SAN with 37.0 mol% acrylonitrile (23.0 mass%, 21.2 vol%) are listed in Table 2 [21,22,24–30]. The properties listed in Table 2 include the molecular weight of the repeat unit, M_0, the density, ρ, the molar volume, v, the glass transition temperature, T_g, the melting point (if applicable), T_m, the heat of fusion (if applicable), ΔH_f, and the solubility parameter, δ. The values of δ from the literature for PEO, PPO, PS and PAN were quite similar to those calculated using the van Krevelen–Hoftyzer group contribution constants [27]. The δ for PCL was calculated using those constants. For SAN, ρ was calculated using a volume fraction rule of mixtures, M_0 and δ were calculated using a mole fraction rule of mixtures, and T_g was calculated using the Fox equation [31] (the T_gs for low molecular weight PS and PAN are listed in Table 2).

In order to provide a basis upon which the miscibilities of the different systems can be compared, polymer–polymer interaction parameters were calculated using two methods. The first method treats SAN as if it was a homopolymer, one component of a two-component blend. The two-component interaction parameter, χ_{ij}, was calculated using Eq. (2). The second method describes blending homopolymer C with a random copolymer containing A and B [32]. The three-component interaction parameter, χ_{ijk}, calculated using Eq. (3), is based upon three χ_{ij}, one for each component pair. The χ_{ij} for the component pairs (χ_{AC}, χ_{BC}, and χ_{AB}) were calculated using Eq. (2). While χ_{ij} will always be positive, χ_{ijk} may also be negative. The interaction parameters were calculated using a temperature, T, of 100 °C (above the mid-block T_m and the SAN T_g). Interaction parameters calculated using temperature of 20 °C were about 30% larger (absolute values).

$$\chi_{ij} = \frac{v_{avg}}{RT}\left(\delta_i - \delta_j\right)^2 \tag{2}$$

$$\chi_{ijk} = \phi_A\chi_{AC} + (1-\phi_A)\chi_{BC} - \phi_A(1-\phi_A)\chi_{AB} \tag{3}$$

where i, j, and k represent different polymers, v_{avg} is the geometric average of the polymers' molar volumes, R is the ideal gas constant, and ϕ_A is the volume fraction of A in the copolymer containing A and B [33].

3.2. Mid-block crystallization

Often, three non-mutually exclusive factors are among the most important influences on the ability of the TBC mid-block to crystallize. In terms of the TBCs these three factors are as follows.

(1) *End-block* T_g. The T_g of SAN is higher than the T_m of the mid-block (Table 2). The presence of SAN in the glassy state, bound to each end of the mid-block, would restrict the mobility of the mid-block and limit its ability to crystallize. TBCs with crystallizable mid-blocks and rubbery end-blocks (an end-block T_g that is less than the mid-block T_m) may behave differently.

(2) *Polymer–polymer miscibility*. In general, homopolymers with similar solubility parameters are less likely to phase separate than polymers with quite different solubility parameters. A self-consistent field phase diagram for the phase-separated nanoscale architectures found in ABA triblock copolymer melts has been described as a function of the interaction parameter multiplied by half the total degree of polymerization (so that there is equivalence with diblocks), here $\chi_{ij}N/2$, and the mole fraction of one of the blocks [34]. The phase diagram includes nanoscale structures (spheres, cylinders, bicontinuous gyroids, lamellae) and a disordered phase [34]. The TBC is disordered, for all compositions, when $\chi_{ij}N/2$ is below 8. The $\chi_{ij}N/2$ for SAN/PEO are all less than 0.2, indicating a relatively miscible system (Table 1). PPO1-a has a $\chi_{ij}N/2$ of 2.9. PCL1-a has a $\chi_{ij}N/2$ of 5.8 and, therefore,

would be the most likely among the three systems to exhibit phase separation. The phase diagram [34] indicates that if a system is close to the order–disorder transition, then increasing the mole fraction of the minor component, increasing the molecular weight, or decreasing the temperature (and, thus, increasing the interaction parameter) could enhance the order in the melt. Changes in the order in the melt can affect the mid-block's ability to crystallize upon cooling [16]. It is also clear that phase separation can be strongly dependent on processing (cooling from the melt, precipitation from a solvent, and drying a cast film can all produce different nanoscale architectures).

The issue is somewhat more complex when treating the TBCs as homopolymer C blended with a random copolymer containing A and B. While the polymer pairs AC, BC, and AB, may all be immiscible and have relatively high interaction parameters, C might be miscible with the random copolymer and even have a negative interaction parameter [35]. χ_{ijk} for SAN/PEO is, in fact, negative, −0.052 (Table 2), indicating a high degree of miscibility. The χ_{ijk} are smaller than the χ_{ij}, but are affected by the mid-block in a similar manner. The interaction parameters are smallest for the PEO mid-block and largest for the PCL mid-block.

(3) *Processing*. The TBCs discussed here have undergone three types of processing, each of which can produce different nanoscale architectures. (a) The as-synthesized materials were precipitated from a solvent (THF) using a non-solvent (methanol). Both the type of solvent and the type of non-solvent affect the nanoscale architecture of the precipitated TBC by affecting which block leaves solution first. (b) Films of the TBCs were prepared by casting from a solvent and drying. In this process, the type of solvent and the drying conditions affect the nanoscale architecture of the TBC. (c) Annealed samples were prepared by cooling from the melt (120 °C).

3.3. Thermal transitions and crystallinity

Thermal analysis of representative homopolymers (SAN1 with 37 mol% AN and M_n 8300 g/mol, PEO1 with M_n 2500 g/mol and PEO2 with M_n 6000 g/mol) yielded typical results. The T_g of the relatively low molecular weight SAN1 (Table 1), 92 °C, is similar to that calculated using the Fox equation (Table 2). The crystallinity of PEO is often in the range of 70% [36]. The crystallinities of PEO1 and PEO2 are 63% and 72%, respectively (Table 1). PEO2, with its higher M_n, exhibits a higher crystallinity. PEO1 and PEO2 have T_m of 56 and 64 °C, respectively (Table 1), similar to the literature value of 66 °C [22]. The higher T_m for the PEO with the higher M_n may reflect a higher degree of order and thicker lamella [37]. PEO has a T_g of −63 °C [24]. It was not possible to discern a PEO T_g in the highly crystalline PEO homopolymers since the crystalline phase restricts the mobility of the amorphous phase.

DSC thermograms from the PEO1-based TBC and the PEO2-based TBC are presented in Fig. 1 and Fig. 2, respectively. DSC thermograms from TBC with various PEO mid-block M_n whose SAN end-blocks have M_n around 5000 g/mol (PEO1-b, PEO2-b, and PEO3-a) can also be compared (Figs. 1 and 2). It was not possible to discern a distinct SAN T_g in any of the TBCs (Table 1) even when SAN was the major component. The absence of a distinct SAN T_g in these TBCs may indicate that the nanoscale structure of the TBC is relatively disordered. It was not possible to discern a distinct PEO T_g in any of the TBC, even when the PEO was the major component and exhibited a relatively low crystallinity (Table 1). Suitable specimens for dynamic mechanical thermal analysis could not be produced since the low molecular weight TBCs were extremely brittle.

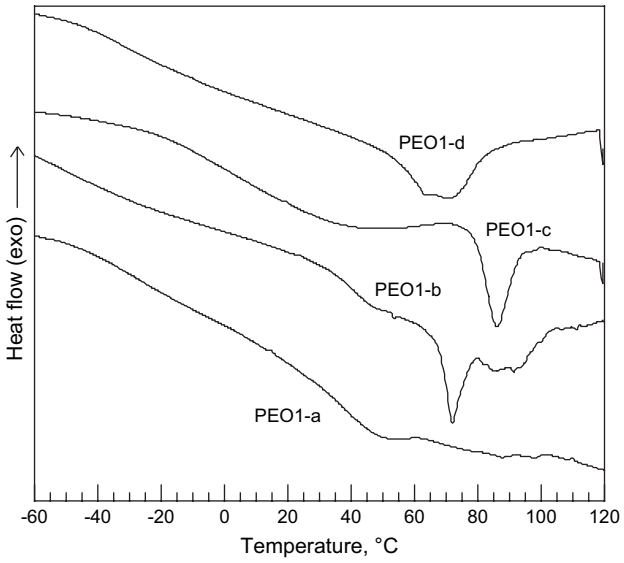

Fig. 1. DSC thermograms of PEO1-a, PEO1-b, PEO1-c and PEO1-d.

The PEO crystallinities in the TBC are significantly lower than those in the homopolymers (Table 1). There is, however, a clear dependence of crystallinity on the molecular weight of the PEO mid-block and on the composition of the TBC. PEO3-a with the highest PEO mid-block M_n (11,500 g/mol) and the highest PEO content (67 mol%) had a relatively

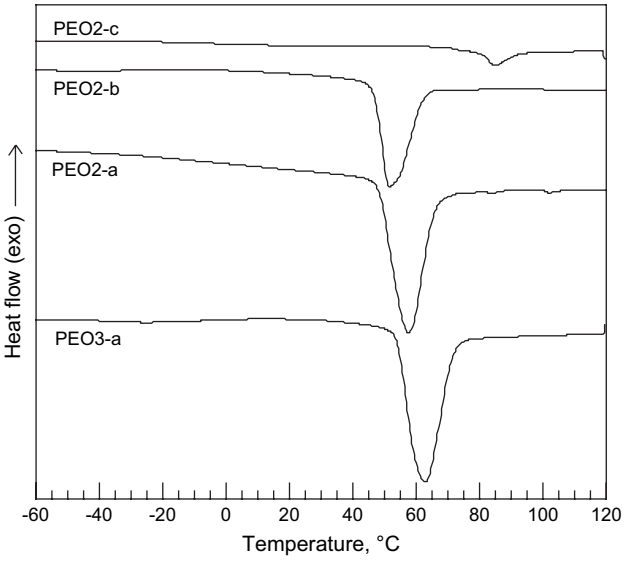

Fig. 2. DSC thermograms of PEO2-a, PEO2-b, PEO2-c, and PEO3-a.

high crystallinity, 38%. The crystallinities of the PEO2-based TBC (PEO M_n of 6100 g/mol) depended strongly on the composition. The PEO2-based TBC with more than 50 mol% PEO, PEO2-a and PEO2-b, also had relatively high crystallinities, 42% and 43%, respectively. The PEO2-based TBC with only 45 mol% PEO, PEO2-c, had a relatively low crystallinity, 12%. This seems to indicate that when PEO is the major component the nanoscale architecture formed is conducive to PEO crystallization. However, when the PEO content drops below 50 mol%, the nanoscale architecture formed severely limits the PEO crystallization.

The crystallinities of the PEO1-based TBC (PEO M_n of 2500 g/mol) are expected to be relatively low since they are limited by the PEO M_n. The crystallinities of the PEO1-based TBC also depended strongly on the composition. The dependence of crystallinity on the composition of the PEO1-based TBCs is the opposite of that seen for the PEO2-based TBCs. The crystallinity of PEO1-a with 43 mol% PEO, a composition similar to that of PEO2-c, is barely discernable, 4% (Table 1). The crystallinity increases as the PEO content decreases, with crystallinities of about 22% for PEO contents of about 20 mol%. The interaction parameter is the same for all the PEO-based TBC, the mid-block molecular weights are identical for all the PEO1-based TBC, and the $\chi_{ij}N/2$ are similar to those in the PEO2-based TBC (Table 1). Therefore, the factor that affects the crystallinity must be the influence of x_{MB} on the nanoscale architecture. x_{MB} decreases from 43% to 18% as the molecular weight of the SAN increases, but the nanoscale architecture formed at low x_{MB} in the PEO1-based TBCs seems to be more conducive to PEO crystallization.

An interesting comparison can be made between the TBCs with similar SAN end-block molecular weights and different PEO molecular weights (PEO1-b, PEO2-b, and PEO3-a). The PEO M_n are 2500, 6100 and 11,500 g/mol and the x_{MB} are 32%, 55% and 66%, for PEO1-b, PEO2-b and PEO3-a, respectively. While PEO1-b exhibits 7% crystallinity, both PEO2-b and PEO3-a exhibit similar crystallinities of around 40%. The 'jump' from a crystallinity of 7% to a crystallinity of 40% must also reflect a change in the TBC nanoscale architecture that is associated with the change in x_{MB} from 32% to 55%. The crystallinity of PEO3-a (38%) is similar to those of PEO2-a (42%) and PEO2-b (43%) since all three TBCs have x_{MB} over 50%.

The PEO TBCs can be divided into two groups based on their crystallinities: TBCs with relatively high PEO crystallinities (PEO2-a, PEO2-b and PEO3-a) and TBCs with relatively low PEO crystallinities (the PEO1-based TBCs and PEO2-c). The TBCs that exhibit relatively high crystallinities have T_ms that are similar to the PEO T_m (Table 1). The similarity in T_m may indicate a similarity in crystalline structure. The PEO T_m of 86 °C (PEO1-c) is similar to the PEO T_m of 85 °C observed for a PAN–PEO diblock copolymer with 13 wt% PEO and observed for other block copolymers [38,39]. The relatively high T_m has been ascribed to the fractional crystallization of imperfect crystals.

The solubility parameters of PEO and SAN are similar, yielding a relatively low interaction parameter (Table 2). For the TBCs with higher N, the tendency to form an ordered phase-separated nanoscale architecture is stronger and the PEO is able to crystallize more readily. This is especially so when PEO is the major component and its mobility is enhanced. Based on $\chi_{ij}N/2$ and x_{MB} the PEO1-based TBCs tend to be disordered. The disorder would limit the ability of the PEO to crystallize, yielding the relatively low X_{MB}. As the M_n of the SAN end-blocks increases in the PEO1-based TBC so does the tendency of the blocks to phase separate and, therefore, so does the ability of the PEO to crystallize. Thus, the PEO crystallinity decreases with increasing SAN M_n in the PEO2-based TBCs and increases with increasing SAN M_n in the PEO1-based TBCs. These conjectures are confirmed through WAXS and SAXS analyses.

3.4. TBC morphology

The thickness of the PEO crystalline lamellae depends upon the molecular weight and crystallization temperature: PEO with molecular weights of less than 3000 g/mol do not ordinarily crystallize in folded chain lamellae, but rather as extended-chain crystals [40]. PEO crystallizes from the melt as very large spherulites containing a large number of lamellae [41]. The typical crystalline length scales in PEO with M_n of 1920 and 2750 g/mol, measured by small angle X-ray scattering (SAXS) and calculated using Bragg's Law, are 130 and 208 Å, respectively [42].

WAXS was employed to characterize the crystalline structure of the PEO homopolymer and the PEO mid-blocks. PEO1 exhibits WAXS peaks at $2\theta = 19.34°$ and 23.46° (Fig. 3 and Table 3) that are typical of PEO and correspond to d-spacings of 4.56 and 3.76 Å, respectively [18]. PEO1 is a monoclinic crystal with a, b, c and β_c of about 8.0, 13.0, 19.5 Å and 125°, respectively [21]. The 4.56 Å spacing represents index (120) and the 3.76 Å spacing represents indices (112) and (032). PEO2 exhibits similar WAXS peaks (Fig. 4 and Table 3).

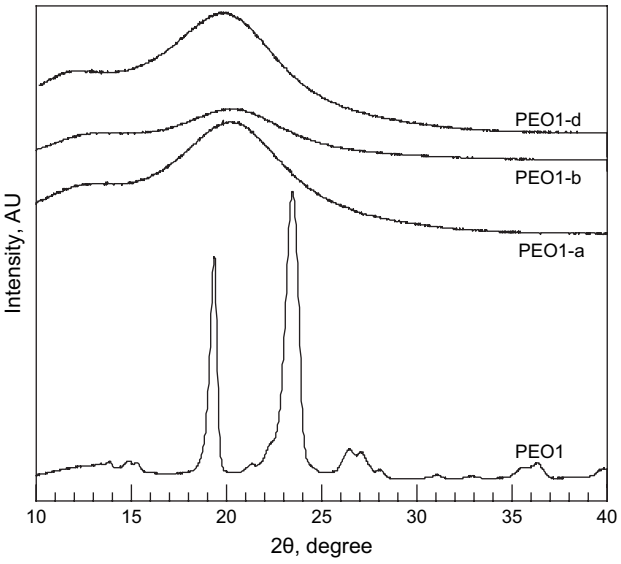

Fig. 3. WAXS of PEO1, PEO1-a, PEO1-b and PEO1-d.

Table 3
Characteristic lengths from WAXS and SAXS

	WAXS		SAXS
	Length (Å)		Length (Å)
PEO1	4.56	3.76	126
PEO2	4.61	3.79	143
PEO2-a	4.49	3.72	170
PEO2-b	4.53	3.75	182
PEO3-a	4.60	3.79	181

PEO2-a and PEO2-b exhibit WAXS peaks similar to those of PEO1 and PEO2 (Fig. 4 and Table 3) indicating crystal structures similar to those of the homopolymers. The relatively high crystallinity and relatively intense WAXS peaks for PEO2-a and PEO2-b indicate the existence of a phase-separated structure in which the PEO can crystallize. WAXS results from TBC with various PEO mid-block M_n whose SAN end-blocks have M_n around 5000 (PEO1-b, PEO2-b, and PEO3-a) can also be compared (Figs. 3 and 4). PEO3-a exhibits intense WAXS peaks similar to those from PEO2-a and PEO2-b indicating the presence of a similar crystal structure. As seen from the DSC crystallinities, when x_{MB} is over 50% the PEO is able to crystallize.

The PEO1-based TBC and PEO2-c exhibit relatively broad WAXS peaks that are typical of amorphous polymers (Figs. 3 and 4). WAXS data from the PMMA sample holder and SAN1 are presented in Fig. 5 (circles). The shoulder in the SAN1 data at about 13° clearly originates in the PMMA sample holder and is only significant in the spectra from amorphous polymers or from polymers with low crystallinities. The WAXS data for the PEO1-based TBCs and PEO2-c are almost identical with the SAN1 WAXS data, as seen for PEO1-d in Fig. 5 (line). There is no evidence of crystalline structure in the WAXS data for these TBCs. These results confirm the conclusions drawn from the DSC analyses. The TBCs can be divided into two types, those with high PEO contents (PEO2-a, PEO2-b and PEO3-a) which exhibit relatively high crystallinities and highly ordered crystalline structures and those with relatively low PEO contents which exhibit relatively low crystallinities and no crystalline order.

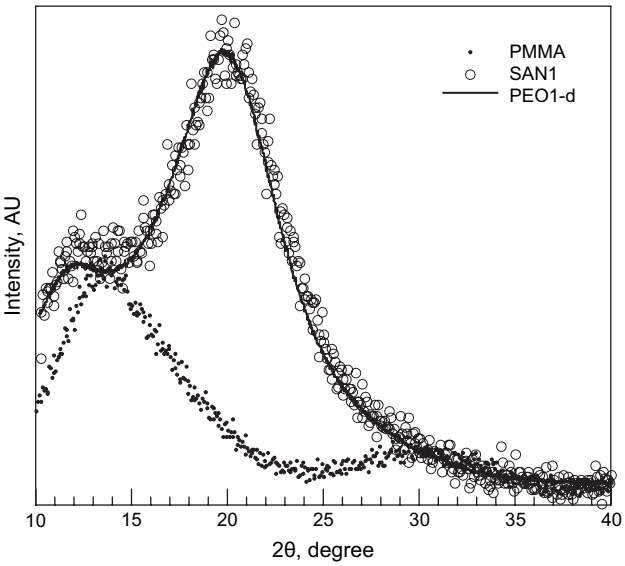

Fig. 5. WAXS of the PMMA sample holder, SAN1 and PEO1-d.

As-synthesized PEO1 exhibits a multiple-peak SAXS pattern (Fig. 6) that is related to a periodicity of 126 Å (Table 3). The PEO2 specimen for SAXS was annealed by heating to 100 °C and then cooling to room temperature in order to eliminate traces of a second set of peaks that appeared in one of the SAXS spectra taken from the as-synthesized PEO2. The annealed PEO2 exhibits a periodicity of 143 Å (Table 3), identical to the periodicity of the main set of peaks seen for the as-synthesized PEO2 (not shown). The 1:2 SAXS peak periodicities in the highly crystalline PEO indicates a lamellar structure consisting of alternating crystalline and

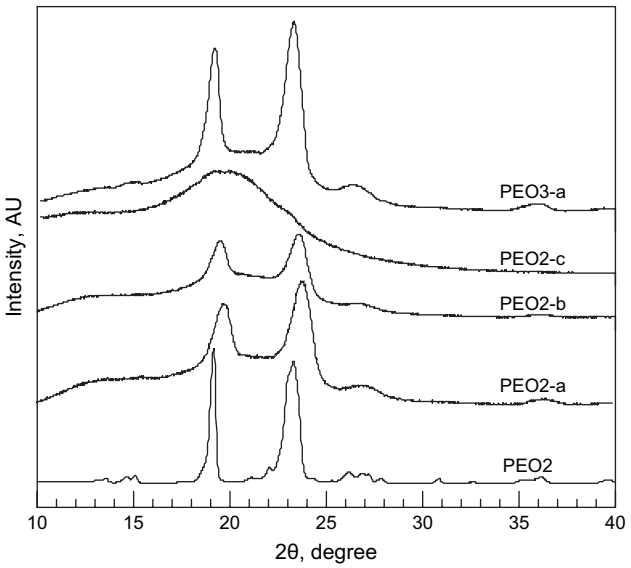

Fig. 4. WAXS of PEO2, PEO2-a, PEO2-b, PEO2-c, and PEO3-a.

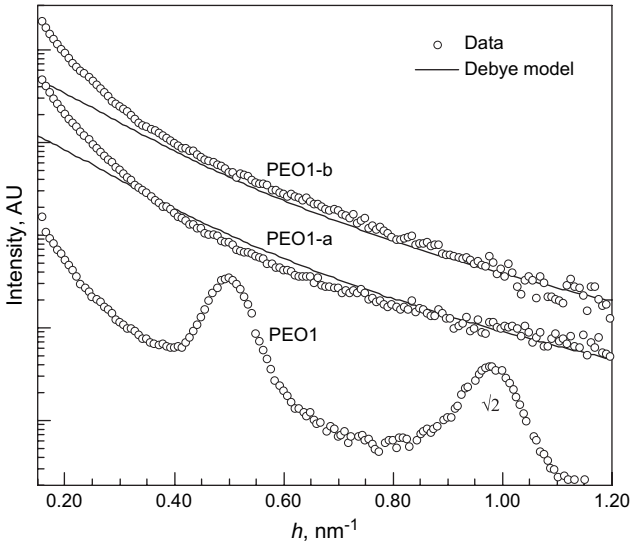

Fig. 6. SAXS data from PEO1, PEO1-a and PEO1-b. PEO1-a and PEO1-b were fit using the Debye correlation function.

amorphous lamellae. Such an alternating crystalline and amorphous lamellar structure is typical of semicrystalline polymers [22]. The higher T_m and the larger lamellar thickness for PEO2 compared to PEO1 can be related to the higher M_n [43]. SAN (not shown) exhibits no SAXS peaks, as expected from an amorphous polymer.

The grouping of the TBCs by their relative crystallinities established through the DSC and WAXS analyses also holds for the analysis of the SAXS results. PEO1-a and PEO1-b do not exhibit the SAXS peaks that are indicative of ordered structures (Fig. 6) and can be fit using the Debye correlation function for disordered, two-phase, non-particulate systems (Fig. 6). The Debye correlation lengths for PEO1-a and PEO1-b are 37.2 and 36.6 Å, respectively. These correlation lengths indicate the existence of relatively small phase-separated structures within which the PEO is not able to achieve long-range order and a high degree of crystallinity.

PEO2-a and PEO2-b exhibit two SAXS peaks that are related to periodicities of 170 and 182 Å, respectively (Fig. 7 and Table 3), larger than the periodicity of 143 Å for PEO2. The 1:2 SAXS peak periodicity for PEO2-a also indicates a lamellar structure. A lamellar structure with a low degree of order can be seen in Fig. 8, a TEM micrograph of a TBC similar to PEO2-a (the M_n of the SAN end-blocks was 3800 g/mol). The layer thicknesses in Fig. 8 are about 60 Å (the periodicity is around 120 Å). The TEM results are consistent with the SAXS periodicities. PEO3-a, with a PEO M_n almost twice that of PEO2 and a crystallinity similar to those of PEO2-a and PEO2-b, exhibits a SAXS periodicity of 181 Å, quite similar to that of PEO2-b (Table 3). The relative insensitivity of the periodicity to the PEO molecular weight seems to indicate that the periodicity reflects the crystalline structure rather than a SAN-PEO phase-separated structure.

The SAXS spectrum from PEO2-a taken at 80 °C (Fig. 7) provides further evidence that the periodicity reflects the crystalline structure rather than a SAN-PEO phase-separated

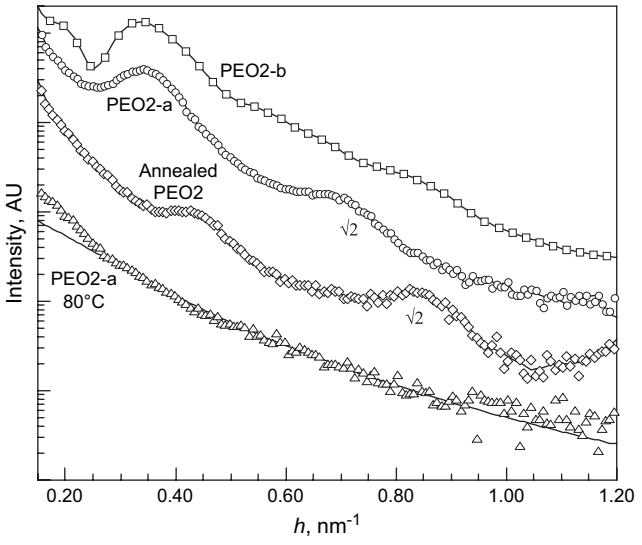

Fig. 7. SAXS from PEO2 (annealed), PEO2-a (as-synthesized and at 80 °C with a Debye correlation function fit) and PEO2-b (as-synthesized).

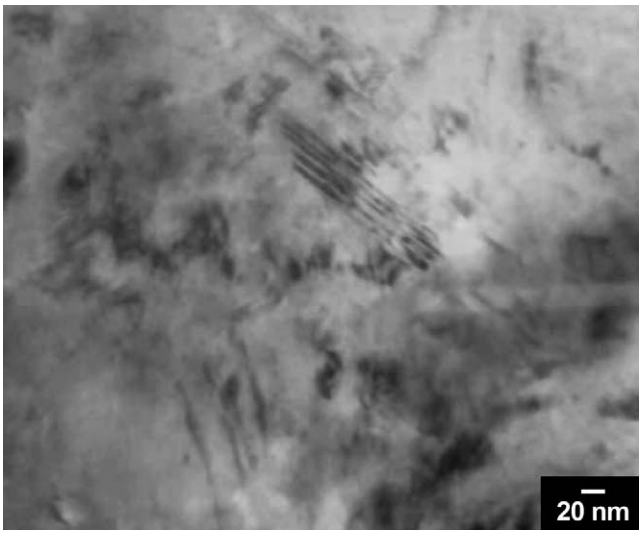

Fig. 8. TEM micrograph of SAN(3800)–PEO(6100)–SAN(3800).

structure. At 80 °C the TBC is above the PEO melting point, but below the glass transition temperature of SAN. All traces of an ordered structure disappear from the SAXS spectrum, which can be fit using the Debye correlation function with a correlation length of 40.1 Å, similar to the correlation lengths for the relatively low crystallinity PEO1-a and PEO1-b which exhibited no ordered structure in WAXS and SAXS. Thus, the lamellar order seen in the as-synthesized TBC disappears upon melting of the mid-block crystallites.

3.5. Effects of mid-block polymer

PPO and PCL are semicrystalline polymers whose T_g and T_m are quite similar to those of PEO, but whose solubility parameters are quite different (Table 2). χ_{ij} for PPO–SAN (0.050) and PCL–SAN (0.099) are significantly higher than that for PEO–SAN (0.0009) (Table 2). It might be expected that the drive to phase separate would be greater in these TBCs in light of their significantly higher χ_{ij}. However, the $\chi_{ij}N/2$ (Table 1), used as a general indicator for the tendency to phase separate, are still relatively low for PPO1-a and PCL1-a (2.9 and 5.8, respectively). In addition, the ability to phase-separate and crystallize in the PEO mid-block TBC has been shown to be strongly affected by x_{MB}. PPO1-a and PCL1-a have relatively low x_{MB} (0.22 and 0.25, respectively) (Table 1).

Typical crystallinities of PPO and PCL homopolymers are 62 and 66%, respectively [44,45]. PPO1-a and PCL1-a exhibit relatively low crystallinities, 26 and 13%, respectively (Table 1). The PPO T_m, 70 °C, is similar to its literature value of 75 °C [21] and the PCL T_m, 58 °C, is similar to its literature value of 60 °C [22]. The T_g of the PCL mid-block is discernable in the DSC thermogram (not shown) at about −50 °C, somewhat higher than the literature value of −62 °C [26]. PCL was the only polymer to exhibit a discernable T_g among the TBC. The WAXS spectra for PPO1-a and PCL1-a (not shown) exhibit the same broad amorphous PMMA/SAN peaks seen for the PEO1-based TBC and PEO2-c and there is no

ordered structure discernable from their SAXS spectra (not shown). These results indicate that for the low molecular weight TBC with low x_{MB}, increasing the interaction parameter was not enough to drive the formation of an ordered phase-separated structure that would enhance crystallization.

3.6. Effects of processing

Annealing has been reported to have significant effects on the nanoscale structure of triblock copolymers [46]. The effects of 'annealing' (the first DSC heat) were characterized by the second DSC heat. Annealing somewhat reduces the PEO homopolymer crystallinity (from 72% to 65% for PEO2) and T_m (from 64 to 60 °C for PEO2). Annealing has a profound effect on the crystallinities of the TBC, eliminating almost all traces of crystallinity, even for PEO2-a with 42% crystallinity as synthesized (Fig. 9 and Table 4). There were no obvious differences in the SEC results for as-synthesized and annealed TBC, indicating that no TBC degradation had occurred.

The almost complete disappearance of crystallinity in all the TBCs indicates a change in their nanoscale architecture. The as-synthesized PEO2-a exhibited a phase-separated PEO nanoscale architecture in which the PEO could crystallize, but upon cooling from 120 °C the PEO was not able to crystallize. The constraint on crystallization is imposed by the reduction in mobility upon cooling as the SAN reaches its T_g of 92 °C. The reduction of mobility prevents the development of a phase-separated nanoscale architecture within which the PEO can crystallize and yields a disordered structure. The lack of a distinct T_g in any of the TBC reinforces the contention that annealing yields a disordered system as opposed to an amorphous miscible blend which would exhibit a distinct T_g.

Casting from a solvent can have significant effects on the nanoscale structure of triblock copolymers that depend on the relative solubilities of the blocks in the solvent. THF and chloroform are solvents for both PEO and SAN. The as-synthesized PEO2 homopolymer has a T_m of 64 °C and a crystallinity of 72%. Casting PEO2 from THF or chloroform yields crystallinities of 64% and 81%, respectively, with relatively insignificant changes in the T_m (Table 4). The WAXS and SAXS spectra for PEO2 cast from THF (not shown) are almost identical to that for as-synthesized PEO2, indicating that casting yields the same crystalline structure.

Table 4
Melting points and crystallinities for annealed and cast PEO2 and PEO2-a

	PEO2		PEO2-a		
	T_m (°C)	X_{MB} (%)	T_g (°C)	T_m (°C)	X_{MB} (%)
As-synthesized	64	72	–	58	42
Annealed	60	65	–	–	0
THF (25 °C)	63	64	−45	53	15
Chloroform (25 °C)	64	81	−47	51	10

The films produced by casting the copolymers have significantly smaller crystallinities than the as-synthesized copolymers. Casting PEO2-a from THF or chloroform reduces the crystallinity from 42% to 15% or 10%, respectively, with similar reductions in the T_m (DSC thermograms in Fig. 10 and Table 4). Casting from THF or chloroform, unlike cooling from 120 °C, can provide enough mobility for the PEO to crystallize. PEO2-a cast from THF or chloroform also exhibits T_gs, −45 and −47, respectively, unlike the as-synthesized TBC. The presence of a distinct, although relatively broad, T_g in the cast PEO2-a may reflect the formation of phase-separated amorphous PEO domains. The WAXS spectra for PEO2-a cast from THF or chloroform (Fig. 11) and the derived lengths of 4.60 and 3.78 Å are quite similar to those of the as-synthesized PEO2-a (Table 3), supporting the DSC results. The spectra do not exhibit a shoulder since the films were cast onto $LiNbO_3$ and the PMMA sample holder was not used.

PEO2-a films cast from THF or chloroform and dried at 150 °C are, essentially, annealed films and exhibit all the

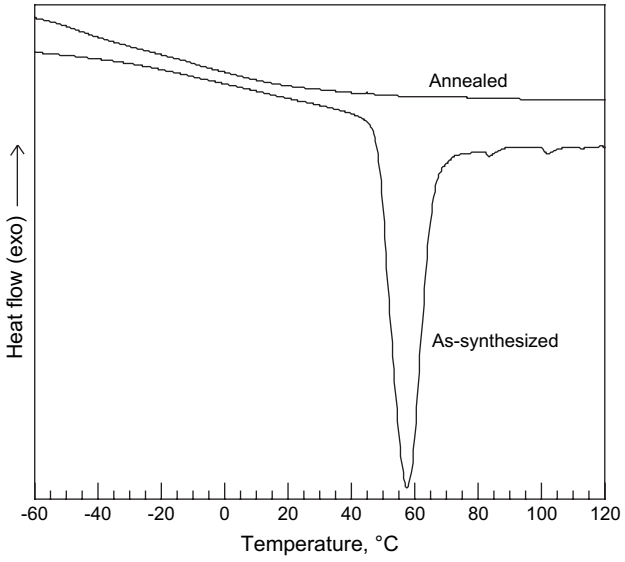

Fig. 9. DSC thermograms of PEO2-a: as-synthesized and following annealing.

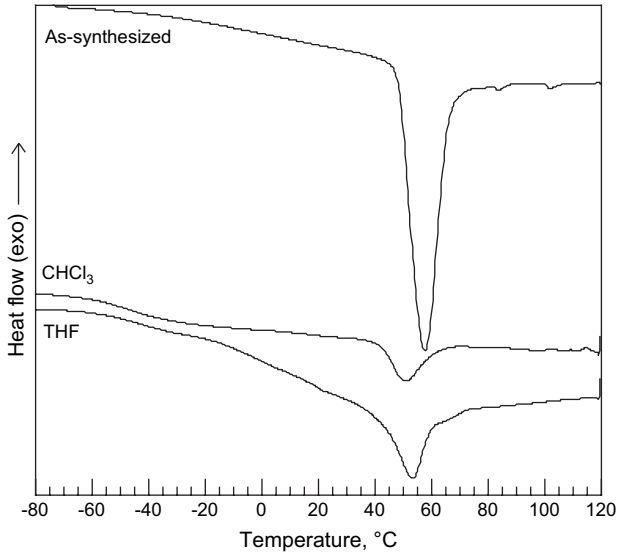

Fig. 10. DSC thermograms of PEO2-a: as-synthesized and following casting (THF or chloroform) and drying at 25 °C.

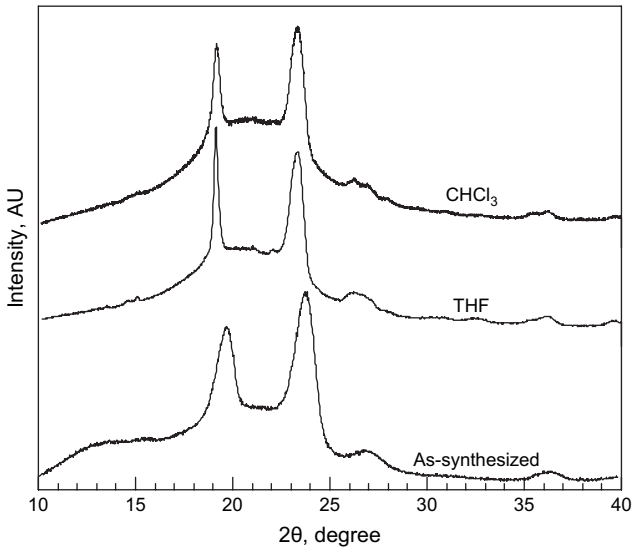

Fig. 11. WAXS of PEO2-a: as-synthesized and following casting (THF or chloroform) and drying at 25 °C.

characteristics of annealed films. The crystallinity in these films is almost entirely eliminated, with DSC and WAXS results (not shown) quite similar to those of as-synthesized PEO1-a in Fig. 1 and Fig. 3. The SAN becomes glassy during cooling from 150 °C and prevents the PEO from crystallizing.

4. Conclusions

Low molecular weight SAN–PEO–SAN, SAN–PPO–SAN and SAN–PCL–SAN triblock copolymers were synthesized and characterized. The influences of molecular weight, composition (mid-block mole fraction), and interaction parameter on the nanoscale structure and crystallinity were studied individually through the synthesis of several sets of TBC materials.

The TBCs with PEO mole fractions above 0.5 exhibited PEO crystallinities of around 40% (compared to 72% for the PEO homopolymer) and lamellar nanoscale periodicities between 170 and 182 Å (compared to 143 Å for the PEO homopolymer). The TBCs with PEO mole fractions below 0.5 exhibited relatively low crystallinities and no ordered structure in WAXS and SAXS. The ability of the mid-block to form an ordered phase-separated structure within which it could crystallize depended more strongly on the mid-block mole fraction than on the molecular weight or on the interaction parameter. The ordered structure originates in the crystalline lamella and, therefore, disappears when a TBC with a relatively high crystallinity was heated to 80 °C, above the PEO melting point but below the SAN glass transition temperature.

The TBC nanoscale structure is significantly affected by processing. It was difficult to discern any crystallinity in the annealed TBC. SAN becomes glassy on cooling from 120 °C, limiting the mobility and, therefore, limiting the ability of the mid-block to crystallize. The crystallinity was reduced from 42%, for the as-synthesized TBC, to 15% or less, for the TBC cast from a solvent and dried at 25 °C. Drying a cast film at 150 °C almost completely eliminated the crystallinity, as seen for the annealed TBC.

Acknowledgements

The authors gratefully acknowledge the partial support of the Binational Science Foundation and the Technion VPR Fund. The authors also gratefully acknowledge A. Siegmann, with thanks for his most helpful discussions.

References

[1] Matyjaszewski K, Davis TP, editors. Handbook of radical polymerization. New York: John Wiley and Sons; 2002.
[2] Wang JS, Matyjaszewski K. J Am Chem Soc 1995;117:5614.
[3] Patten TE, Xia J, Abernathy T, Matyjaszewski K. Science 1996;272:866.
[4] Matyjaszewski K, Xia J. Chem Rev 2001;101:2921.
[5] Kamigaito M, Ando T, Sawamoto M. Chem Rev 2001;101:3689.
[6] Hawker CJ, Bosman AW, Harth E. Chem Rev 2001;101:3661.
[7] Matyjaszewski K. Prog Polym Sci 2005;30:858.
[8] Patten TE, Matyjaszewski K. Adv Mater 1998;10:901.
[9] Matyjaszewski K. Prog Polym Sci 2005;30:858.
[10] Davis KA, Matyjaszewski K. Adv Polym Sci 2002;159:2.
[11] Matyjaszewski K, Xia J. In: Matyjaszewski K, Davis TP, editors. Handbook of radical polymerization. New York: John Wiley and Sons; 2002. p. 527.
[12] Kowalewski T, Tsarevsky NV, Matyjaszewski K. J Am Chem Soc 2002;124:10632.
[13] Tsarevsky NV, Sarbu T, Gobelt B, Matyjaszewski K. Macromolecules 2002;35:6142.
[14] Cohen Y, Albalak RJ, Dair BJ, Capel MS, Thomas EL. Macromolecules 2000;33:6502.
[15] Walker TA, Semler JJ, Leonard DN, Maanen GJ, Bukovnik RR, Spontak RJ. Langmuir 2002;18:8266.
[16] Koo CM, Wu L, Lim LS, Mahanthappa MK, Hillmyer MA, Bates FS. Macromolecules 2005;38:6090.
[17] Lim LS, Harada T, Hillmyer MA, Bates FS. Macromolecules 2004;37:5847.
[18] Cho I, Kim JB, Jung HJ. Polymer 2003;44:5497.
[19] Tsarevsky NV, Matyjaszewski K. Macromolecules 2002;35:9009.
[20] Hall IH. Structure of crystalline polymers. New York: Elsevier Applied Science; 1984. p. 283–9.
[21] Miller RL. In: Brandrup J, Immergut EH, Grulke EA, editors. Polymer handbook. 4th ed. New York: John Wiley and Sons; 1999. p. VI-1.
[22] Nava D, Sakin C, Prolongo MG, Masegosa RM. J Mater Process Technol 2003;143–144:171.
[23] Glatter O. Acta Phys Austriaca 1977;47:83.
[24] Andrews RJ, Grulke EA. In: Brandrup J, Immergut EH, Grulke EA, editors. Polymer handbook. 4th ed. New York: John Wiley and Sons; 1999. p. VI-193.
[25] Grulke EA. In: Brandrup J, Immergut EH, Grulke EA, editors. Polymer handbook. 4th ed. New York: John Wiley and Sons; 1999. p. VII-675.
[26] Orwoll RA. In: Mark JE, editor. Physical properties of polymers handbook. New York: American Institute of Physics; 1996. p. 81.
[27] van Krevelen DW. Properties of polymers. New York: Elsevier; 1990 [chapter 7].
[28] Schrader D. In: Brandrup J, Immergut EH, Grulke EA, editors. Polymer handbook. 4th ed. New York: John Wiley and Sons; 1999. p. V-91.
[29] Korte S. In: Brandrup J, Immergut EH, Grulke EA, editors. Polymer handbook. 4th ed. New York: John Wiley and Sons; 1999. p. V-59.
[30] Runt JP. In: Mark HF, Bikales NM, Overberger CC, Menges G, editors. Encyclopedia of polymer science and engineering. 2nd ed, vol. 4. New York: John Wiley and Sons; 1989. p. 487.
[31] Sperling LH. Introduction to physical polymer science. 2nd ed. New York: John Wiley and Sons; 1992.

[32] ten Brinke G, Karasz FE, MacKnight WJ. Macromolecules 1983; 16:1827.
[33] Krause S. In: Paul DR, Newman S, editors. Polymer blends, vol. 1. New York: Academic Press; 1978.
[34] Matsen MW, Thompson RB. J Chem Phys 1999;111:7139.
[35] Merfeld GD, Paul DR. In: Paul DR, Bucknall CB, editors. Polymer blends, vol. 1. New York: Wiley-Interscience; 2000. p. 70.
[36] Hussain H, Budde H, Horing S, Busse K, Kressler J. Macromol Chem Phys 2002;203:2103.
[37] Wunderlich B. In: Turi A, editor. Thermal characterization of polymeric materials. New York: Academic Press; 1981. p. 183–4.
[38] Sui K, Gu L. J Appl Polym Sci 2003;89:1753.
[39] Nagarajan S, Srinivasan KSV. J Polym Sci Part A Polym Chem 1995; 33:2925.
[40] Ashman PC, Booth C. Polymer 1975;16:889.
[41] Allen G, Tanaka T. Polymer 1978;19:271.
[42] Fraser MJ, Cooper DR, Booth C. Polymer 1977;18:852.
[43] Hong S, Yang L, MacKnight WJ, Gido SP. Macromolecules 2003;34:7009.
[44] Fogliato M, Lima S, Zen Vasconcellos MA, Samios D. J Polym Sci Part B Polym Phys 2002;40:896.
[45] De Kesel C, Lefèvre C, Nagy JB, David C. Polymer 1999;40:1969.
[46] Tanaka S, Ogura A, Kaneko T, Murata Y, Akashi M. Macromolecules 2004;37:1370.